NUCLEATION AND GROWTH ON DEFECT SITES:

Experiment-theory comparison for Pd/MgO(001)

J. A. Venables[1,2]*, L. Giordano[3] and J.H. Harding[4]

1) Department of Physics and Astronomy, Arizona State University, Tempe AZ 85287, USA

2) School of Science and Technology, University of Sussex, Brighton BN1 9QH, UK

3) Dipartimento di Scienza dei Materiali, Università di Milano-Bicocca, 53-20135 Milano, Italy

4) Department of Engineering Materials, University of Sheffield, Sheffield S1 3JD, UK

Abstract

It is well established that nucleation of metal clusters on oxide and halide surfaces is typically dominated by defect sites. Rate equation models of defect nucleation have been developed and applied to these systems. By comparing the models with nucleation density experiments, energies for defect trapping, adsorption, surface diffusion and pair binding have been deduced in favourable cases, notably for Pd deposited on Ar-cleaved MgO(001). However, the defects responsible remain largely unknown. More recently, several types of *ab-initio* calculation have been presented of these energies for Pd and related metals on MgO(001) containing several types of surface defects; these calculated values are surveyed, and some are widely divergent. New rate equation nucleation density predictions are presented using the calculated values. Some calculations, for some defect types, are much closer to experiment than others; the singly charged F_s^+ centre and the neutral divacancy emerge as candidate defects. In these two cases, the Pd/MgO(001) nucleation density predictions agree well with experiment, and the corresponding surface defects deserve to be taken seriously. Energy and entropy values are discussed in the light of differences in calculated charge redistribution between the metal atoms, clusters and (charged) surface defects, and (assumed or calculated) cluster geometries.

*Corresponding author. Tel: (480) 965-1675; Fax: -7954; Email: john.venables@asu.edu

PACS Numbers: 68.43;68.55;71.15;73.20;81.15;82.20;82.65. Keywords: Vapour growth; Defect site nucleation; metals on ionic crystals; Pd/MgO(001), *ab-initio*, DFT and cluster calculations

Accepted for J. Phys. Cond. Matter (August 2005). *Version 13 October, ex 23 August 2005*

1. Introduction

Thin metal clusters supported on oxide surfaces have many practical applications due to their catalytic, magnetic and electric properties; experiment and theory have given rise to a large literature [see, e.g.1-3]. A few years ago, two of the present authors were involved in trying to understand experiments on defect-induced nucleation of metal growth on alkali halide surfaces [4], and on alkaline earth oxides [5], the most recent experiments having used atomic force microscopy (AFM) [6]. A rate equation treatment showed that several energies associated with defect-influenced nucleation and growth can be determined, for the specific case of Pd/MgO(001); some calculations were done [5, 6] to compare energy values with experiment. This rate equation treatment is briefly reviewed in section 2.

In recent years, quantum calculations of the binding of metal atoms and clusters to oxide and halide surfaces have progressed, giving a stimulus for experimental determination of interaction parameters. Several groups have presented calculations of relevant energies for several metal deposits, including Pd, Pt, Ag and Au on MgO and NaCl, over the last few years. However, as we discuss in section 3, the results have been rather widely discrepant; there are also several types of surface defects to be considered as candidates for nucleating agents. We tabulate some of these results, comment on the level of agreement, and give possible reasons for discrepancies, centering on the role of charge redistribution at surface defects. Finally, in section 4, we present new rate equation calculations using selected calculated energies for specific surface defects, in the case of Pd/MgO(001), to illustrate the range of experimental predictions and to discuss the way forward. Two particular surface defects, the F_s^+ vacancy and the neutral divacancy, emerge as candidate defects that deserve to be taken seriously in future.

2. Rate equation models of defect-influenced nucleation

Rate equations have been developed to analyse nucleation and growth on perfect substrates over a number of years [7-9]. Defects have been incorporated at the cost of at least two additional material parameters, the trap density n_t, and the trap energy E_t; this also involves doubling the number of rate equations, as both trapped and free species must be considered in parallel. These developments have been reviewed recently in the context of quantum dots [10] and the early stages of thin film growth [11].

Here we give a qualitative account and some examples. We focus on the rate equation for the nucleation density, where the traps are attractive surface point defects, in the simplest case where just one type of trap is present, and that dimers and larger clusters can neither diffuse, nor leave the traps. Within this model, we then estimate trapping and other energies by comparison with experiment, as applied to Pd/MgO(001).

2.1 Rate equation models for perfect substrates

There are two extreme ways of using rate equations to estimate the nucleation density of clusters on substrates. In previous work it has been shown that the important material parameters can be isolated by dividing the clusters sharply into three categories: single mobile adatoms, sub-critical clusters, and absolutely stable clusters [7-9]. Steady-state conditions apply approximately after a short time, where the adatom concentration is constant; then the concentration of critical clusters, which can be evaluated using local equilibrium arguments, yields the nucleation rate and maximum cluster density.

By these means the (in-principle infinite) set of ordinary differential equations (ODEs) can be reduced to a coupled pair of non-linear algebraic equations for the adatom density n_1 and the maximum or saturation density n_x of 2D or 3D stable clusters. Coupled to a suitable growth equation, dependent on cluster shape, these two densities can be calculated as a function of the deposition flux, F (or rate R in the older literature), and substrate temperature T. The critical nucleus size i and the regime of condensation are both determined self-consistently as an output of an iterative calculation for given input adsorption (E_a), diffusion (E_d) and binding (E_b) energies [7-11]. In these calculations, lateral pair binding is typically assumed, so the cluster binding energy (E_i) is made up of the number of lateral bonds in the cluster (b_i) as $E_i = b_i E_b$. However, this restriction is not required, we simply (*sic!*) need to know the energies of all clusters E_j that *could possibly be* the critical cluster. Needless to say, such energies are *not* known in the general case, making the lateral pair-binding model the best starting point in the absence of further information. We modify this approach here in section 4, in the light of recent theoretical estimates described in section 3.

Alternatively, the full time-dependence can be retained, and the coupled ODEs solved with the dose θ (or deposition time, t, where $\theta = Ft$) as the independent variable. This again is simple in principle. But the problem is that we really do need to know all energies and pre-exponential factors in order to calculate anything concrete, except in the case of $i = 1$, when (D/F) is often

the only important parameter. These unknown factors include the frequency associated with the adatom diffusion constant D, as well as the various capture numbers σ that self-consistently determine the reaction rates on the surface. The net result is that this method has been attempted only in a few cases where there is a hope of identifying the corresponding processes by experiment. Typically, the important parameters are lumped rather than elementary quantities; the algebraic method is well suited to identifying such parameters in specific cases.

2.2 Extension to nucleation on defects

Nucleation on point defects can be visualised schematically as in Figure 1, where we separate the adatoms and clusters on the traps (n_{1t} and n_{xt}) from those on the perfect terrace (n_1 and n_x). New nucleation can occur at both perfect and defect sites, but for attractive defects, the numbers are biassed in favour of the latter. We can see this via the rate equation for trapped adatoms, which can be written [5, 6]

$$dn_{1t}/dt = \sigma_{1t} D n_1 n_{te} - n_{1t} \nu_d \exp(-(E_t+E_d)/kT), \quad (1)$$

where n_{te} is the number of empty traps = $(n_t - n_{1t} - n_{xt})$ and σ_{1t} is the capture number of traps for adatoms. After a short time, dn_{1t}/dt reaches a steady state value of zero; inserting the usual expression for the diffusion constant $D = (\nu_d/4)\exp(-E_d/kT)$ in monolayer (ML) units, we deduce

$$n_{1t}/(n_t - n_{xt}) = A/(1+A), \text{ with } A = n_1 C_t \exp(E_t/kT), \quad (2)$$

where $C_t = \sigma_{1t}/4$ is an entropic constant, set equal to 1 in the published calculations to date. This equation (2) shows that the traps are full ($n_{1t} = n_t - n_{xt}$) in the strong trapping limit, whereas they depend exponentially on E_t/kT in the weak trapping limit, as expected. This is thus a Langmuir-type isotherm for the occupation of traps; the trapping time constant to reach this steady state is very short unless E_t is very large; but if E_t is large, then the traps are full anyway.

The total nucleation rate is the sum of the nucleation rate on the terraces and at the defects. The nucleation rate equation becomes, without coalescence,

$$dn_x/dt = \sigma_i D n_1 n_i + \sigma_{it} D n_1 n_{it}, \quad (3)$$

where the second term is the nucleation rate at defects, and n_{it} is the density of critical clusters attached to defects, σ_{it} being the corresponding capture number. The two terms on the right hand side of (3) are in the ratio $B_t = 1 + A_t$. As argued in somewhat more detail elsewhere [10, 11], in the simplest case where the traps only act on the first atom which joins them, and entropic effects are ignored, we have

$$A_t = n_{1t}/n_1 = (n_t - n_{xt})A/[n_1(1+A)]. \quad (4)$$

The model is completed by using links (2) and (4) betwen A_t, A, and n_1 in the modified algebraic equation for n_x, resulting in published curves [5, 6] repeated here in figures 2 and 3 for clarity. Figure 2 shows the behavior for a large T range, for $n_t = 2.65\text{x}10^{-3}$ ML, $E_t = 1.5$ eV, E_b and $E_a = 1.2$ eV, and E_d in the range 0.2-0.4 eV, with a value of $\nu_d = 3$ THz; this is the value that is consistent with the vapour pressure of bulk Pd; we return to this topic in section 4. Comparison with Pd/MgO(001) AFM experiments [6] allowed several energies to be deduced. To reproduce the long plateau region, where $n_x = n_t$, the trapping energy E_t has to be high, ≥ 1.5 eV, as shown in figure 3(a), and the diffusion energy E_d must be low, ≤ 0.3 eV (figure 2). A low value of E_d is needed so that the adatoms can migrate far enough at low T to reach the defect sites before forming stable pairs. This low-T case is discussed further in section 4.

With such a high value of E_t, something else eventually intervenes at high T. This feature is addressed in figure 3(b). Venables and Harding [5] explored two possibilities, assuming that an ad-dimer forms a stable pair at least up to $T \cong 600$ K: one possibility is that condensation becomes incomplete at this point, but that pairs remain stable, $i = 1$. This would indicate a lower limit to the value of E_b, with a moderate value of E_a being the important parameter. The other possibility was the inverse, where the first process that intervenes is the transition to $i = 3$ (as a consequence of the pair-binding model in the square (001) geometry, see inset in figure 2), i.e. the high-T data determines E_b, and only at yet higher T is condensation incomplete. Thus the limiting process becomes the breakup of the cluster (on a trap), rather than removal of the adatom from the trap. The value of E_t was shown not to be important, provided it is high enough.

These two possibilities had different consequences for other measurements in the high T region; in particular the condensation coefficient is very different for the two cases [5, 6]. Incomplete condensation was observed via AES measurements (triangles in figure 2), and the flux-dependent island density measurements [6] were also in agreement only with the second case. Figure 3 indicates that $i = 1$ at low T, but that the transition to $i = 3$ is responsible, within the model, for the initial drop-off at high T, followed by incomplete condensation at the highest T for a good fit. The plots with $E_d = 0.2$ eV correspond to the ‘best fit’, added in figure 2, indicate that both E_a and E_b are around 1.2 eV. Note that the value of E_b is an “effective” value implied by the pair-wise additive model employed; we return to this point in section 4.

3. Recent calculations of relevant energies

3.1 Classical atomistic simulation on perfect MgO(001) substrates

There are many schemes used to calculate interaction energies, which can then be used to relate the above "experimental" values to *ab-initio* theory, and several papers have addressed this issue since the experiments and first models [5, 6] were published. Two of the present authors [5] used classical atomistic simulation to calculate the energies E_a, E_d and E_b and some defect parameters, which assumes that the interactions between atoms and ions can be described using a central-force pair potential.

The interaction between the metal atoms and the ions was first calculated within the Dirac-Fock approximation, using suitable wave functions. It is important to calculate the oxide wave functions using a local potential to represent the effects of the lattice, because the O^{2-} ion is not stable in free space. Then estimates for the correlation and dispersion terms were added. Metal polarizability was included in the shell model. Interactions between metal atoms in the dimer were fitted to a Morse potential, resulting in potential parameters given in equations 5 for Pd_2 [12] and 6 for Ag_2 [13]

For Pd_2: $V(r) = 1.220\ [eV]\ (1 - \exp(1.42018\ [Å^{-1}]\ (\ 2.4800\ [Å] - r\ )))$; (5)

For Ag_2: $V(r) = 1.784\ [eV]\ (1 - \exp(1.43511\ [Å^{-1}]\ (\ 2.5303\ [Å] - r\ )))$. (6)

At that time, some local density approximation (LDA) calculations were available for the simpler configurations [14-16], and comparison with [5] is shown in Table I. The biggest discrepancy is for Pd over the Mg^{2+} site; however, the LDA calculations had a rather large basis-set superposition correction which reduced their accuracy. Overall the agreement is remarkably good, given that it is certainly unreasonable to claim absolute accuracy < 0.1 eV. Venables and Harding [5] also calculated the behavior of monomers and dimers. This enabled them to compare the adsorption and diffusion energies, which are shown and compared with early DFT values in Table II. From this body of work we can be fairly clear that the diffusion energy for both Pd and Ag is rather low, implying rapid adatom diffusion at all temperatures studied experimentally [6].

3.2 Calculations of adatom adsorption, defect trapping and pair-binding

Since this work several papers have been published using a variety of methods, and most recently these have considered trapping at an increasing array of surface defects. The first paper

was a cluster calculation that specifically considered the charge state of surface vacancies [17]; we return to this paper along with more recent papers from the same group later in section 3.3.

The next papers were several sets of Density Functional Theory [DFT] calculations, including the Generalized Gradient Approximation [GGA] extension, of adsorption, trapping and pair-binding energy values for several noble and transition metals [18, 19, 20]. The first of these was an update of reference [14], with revised energy values for Cu, Ag, Ni and Pd [18] in F_s and F_s^+ centres. The second [19] was a study of Pt, and the third studied several noble and transition metal elements [20]. Here, we focus on the small square of the periodic table containing Pd, Pt, Ag and Au, and comment on the values obtained for E_a, E_b and the trapping energies E_t (monomers) and of E_{2t} (dimers) at a particular type of surface vacancy, the F_s centre. This centre is caused by removing a neutral oxygen atom, and hence contains two electrons trapped near the vacancy at the MgO(001) surface. This last paper also commented on possible interpretations of experiments on Pd/MgO [6]; we return to this topic in section 4.

The study of Pt/MgO(001) [19] showed that the trapping energy of Pt at the F_s centre was rather large. In the wide-ranging paper that followed [20], the same methods were used to study several transition metals and a single type of defect trap, in an attempt to generalize the implications. Some of these values are reproduced in Table III. The authors note that the metal atoms are strongly bound to the (charge neutral) F_s centre, because the metal atoms trap electrons from the neighbourhood of the vacancy, leading to a strong surface dipole. This effect was calculated to be very strong for Pd and Pt, and less strong but still sizeable for Ag and Au. The same effect is at work in weakening the pair bond of Pd_2 and Pt_2 from their free space values, most extremely in the case of Pd_2, which was estimated to be unbound on the perfect surface and almost unbound at the defect site. Note also that the calculated adsorption energies E_a for Pd and Pt are high, higher than the value for Pd in table II, but bracketing the "experimental" value of ref. [6]; but for Ag the situation is reversed, arguably within error, which is probably around ±0.2 eV. Note also that the terrace adsorption energy E_a, and trapped atom energy E_t are very similar in refs [18] and [20] for the two elements Pd and Ag that are in both studies; this point was not noticed in ref [20], but does corroborate their basic calculation of single adatom energies.

There are some other trends exhibited in Table III, and we comment on these in this paragraph. First, while the trapping and pair binding energies for Pd and Pt imply a large

electron transfer to adatoms and pairs from the defect site, the transfer must be much less for Ag and Au. Indeed the calculated pair binding energies for the two noble elements in [20] on the MgO(001) surface are almost the same as the free space values. These are known experimentally for Ag_2 = 1.65 ±0.06 and Au_2 = 2.29 ±0.02 eV [21, 22]; for Pd_2 a much wider spread of experimental values has been reported, covering a huge range from 0.73 to 1.69 eV [5]; all empirical work and most calculations prefer the lower end of the range, with all calculations below 1.35 eV [5, 21-26], with the value of 1.22 eV used by two of the present authors in ref [5]. For Pt_2 the experimental value quoted in ref. [19] is 3.70 ±0.16 eV to be compared with the authors' calculated value of 3.64 eV. Thus the authors of ref. [20] have obtained a sizable trapping energy for the monomers of all these metals, while finding a weakened pair binding only for the transition metals (Pt_2 and especially Pd_2), but not for the noble metals (Ag_2 and Au_2). We return to this topic in section 3.3.

Another point is that the diffusion energy for Pd on MgO(001), mentioned only in passing in [20], is given as E_d = 0.86 eV. We did not know how the authors obtained this value, other than possibly by assuming a diffusion path that goes over the Mg^{++} site. As we can see by comparison with Figure 2, this value is much too large to agree with experiment. Moreover, the geometries of almost all the pairs, including Pd_2 and Ag_2, stick out from the surface [20], whereas other calculations, including our own, have them lying in the surface plane. We spell this out in more detail later, but this suggests an unwanted dipole field perpendicular to the surface in that calculation. The above arguments suggest that relatively long range electric fields may not have been adequately relaxed. Or is it the case that the long range (radial) relaxation cannot be properly included in periodic boundary condition DFT-GGA calculations [19, 20], a problem that may be particularly troublesome for ionic crystals.

3.3 Embedded clusters and periodic slabs: small Pd and Ag particles at surface defects

Cluster calculations have a long history, and great credit is due to the Pacchioni group for having been the first to draw attention to the role of the charge state of the defect as a major player in the energies of metals at surface defects. In a clear and informative early paper [17] they gave unambiguous definitions of the F_s, F_s^+ and F_s^{++} as well as the corresponding V_s centres. They calculated that the neutral F_s centre, with 2 electrons at the vacancy, binds Pd by 1.55 eV, whereas Ag, and the alkali atom Rb, were unbound. The F_s^+ centre, with 1 electron, binds both Pd with E_t = 0.77 and Ag with 0.99 eV. The F_s^{++} centre with no electrons ionizes

both Pd and Ag to give Pd^+ and Ag^+; these species are unbound to the resulting F_s^+ centre. All these (Hartree-Fock based) results were however obtained from relatively small MgO clusters, embedded in an array of fixed point charges, so long-range relaxation is an issue.

The Ag and Pd atoms were found to be essentially unbound on the "perfect" surfaces, with E_a <0.01 eV for Ag and E_a = 0.11 eV for Pd on the O^{2-} site; these values are too low. The group's first relativistic DFT calculations gave E_a = 0.20 eV for Ag, 0.23 eV for Au, 0.81 eV for Pd and 1.36 eV for Pt [14]. These values were updated for Pd and Ag [18] as given in Table III alongside for the DFT-GGA slab calculations [19, 20]; there is thus now basic agreement between different DFT calculations. It is also notable that other HF-based calculations of E_a for Ag are very low (~0.20 eV), with E_d even lower (~0.05 eV) [27]. It is not clear what the errors are, but the authors feel that these calculated values are rather too low, for example by comparison with those given in Table II [5] and Table IV [18, 28, 29] which follows.

The next three papers from the group compared two types of DFT-GGA calculations, embedded cluster models and periodic supercells, for Pd, Pd_2 and for small Pd clusters on MgO(001) [28-30]. All calculations are spin-polarised, allowing for magnetic states to emerge, enabling the authors to distinguish the triplet ground state (d^9s^1) of Pd and Pd_2 in the gas phase from the singlet ground state (d^{10}) on the surface. Despite the publication date order, [29] was completed first, and some of the work is described as preliminary; this paper has effective core potentials for the Mg^{++} ions surrounding the cluster within an outer array of fixed point charges; thus, when there is a difference, values from [28, 30], which use a more sophisticated intermediate region of 900 classical polarisable ions [31], are quoted.

The two sets of DFT energies are closely comparable, and several types of defect were considered: F_s and F_s^+ centres, divacancies and steps. Selected periodic supercell energy values [28] are given in Table IV, alongside cluster (BP-level) calculations [28, 29], and cross-checked where possible with [18]. We refer the reader to these papers for further details and caveats on the methods, all of which relate to the ultimate accuracy that one can expect; we will be very fortunate if values hold up to ±0.1 eV, so no significance should be attached to the second decimal place. An important point highlighted in [29] is that the discrepancy between their binding energy for Pd_2, (E_b = 0.46-0.57 eV depending on the details) and that the previous DFT calculations [20] of the same quantity (E_b = –0.03 eV) is the very different geometric

configuration of the stable dimer. In [20, table 2] almost all dimers were strongly angled to the surface plane, with the height of the second atom considerably greater than the first. The relaxation path of the dimer was symmetry restricted along the path towards the cation site, at variance with the stable orientation found in both refs [5] and [28-29], where the dimer axis lies closely in the surface plane with both Pd atoms over the oxygen sites. Thus we attribute the discrepant values for dimers in Table III as being due to, or at any rate correlated with the choice of geometry, coupled with a symmetry-restricted calculation.

In the third paper, one of the present authors produced calculations on Pd nanoclusters [30]. These calculations were able to go far beyond the limited experimental constraints of ref [6], and deduce both configurations and energies of small Pd clusters Pd_n up to n = 4. At the F_s centre, Pd_2 has the minimum binding energy 0.57 eV, whereas Pd_3 is bound by a further 0.75 eV and Pd_4 by another 1.38 eV [30]. It is notable that these values are approaching the value for bulk Pd from below. There is a huge amount of detail in this paper, much more than we can summarize here. In particular, we note that the monomer diffusion energy on the terrace is given as E_d = 0.34 eV as against 0.23 eV [15], close to the upper limit value deduced from experiment [6]. Subsequently, we checked the possibility that the other previous value of E_d = 0.86 eV [20] corresponded to an assumed migration path over the Mg^{++} site. We checked personally [39], and also repeated the slab calculation [30], obtaining 0.82 eV. This confirms that the adatom properties are very similar in refs [20, 28 and 30]; the cluster properties however differ, as discussed above.

4. Further rate equation predictions using calculated energies

4.1 New features of rate equation predictions

In this section we return to the rate equation treatment described in section 2, and show some predictions for nucleation densities using the theoretical energies discussed in section 3. The previous treatment was formulated in term of a simplified model, where cluster bonds were assumed to be given in terms of lateral pair bonds of strength E_b; when defect trapping is involved, it was characterised by a single, additive, trapping energy E_t. However, as mentioned earlier, this is not an inherent restriction: provided we know the energies E_j of all *j*-clusters to be considered as potential critical clusters, then the calculation can be performed explicitly. The energy calculations of ref. [30] for all such clusters Pd_n for n up to 4, makes such a prediction

worthwhile. We are not looking here for exact agreement with experiment, because inputting specific but uncertain (energies/kT) into exponents is bound to give quite large variations in the numerical predictions. For the same reason, we round the energy values to the nearest 0.05 eV.

Since the publication of refs 5 and 6, the relevant nucleation density program has been converted from Fortran into MatLab®6.5 as described elsewhere [10]. This makes no difference in principle, but graphic output can be inspected in real-time, and the code is more user-friendly. In particular, all inverse temperatures (T^{-1}) and all cluster sizes (j) considered can be addressed simultaneously as a single matrix in one-line statements. Given that the defect nucleation program starts from the solution for the density on the perfect substrate, and is iterated to the defective substrate solution, one can easily follow how the density values are changing, and where one might wish to alter convergence parameters. The T^{-1} range, density of T^{-1} points, j-clusters considered, energies and lateral bond parameters (b_j) are all specified in a single input file. General binding energy values for the various clusters are simply included by non-integral values of b_j.

Otherwise, all the features of the previous calculation, including the Einstein model of vibrations, with the same frequency factors, appropriate for bulk Pd, are preserved. Equally, these pre-exponential parameters can be easily changed to judge the extent that such minor parameters influence the predicted nucleation density.

4.1 Nucleation predictions for F_s, F_s^+ and divacancy traps

Figures 4-6 show the high temperature region of the Arrhenius plots, for the same T^{-1} range as figure 3, to explore the predictions for the F_s, F_s^+ and divacancy traps. These figures show the effect of the diffusion energy in the range 0.2-0.4 eV in steps of 0.05 eV, but with all other energies as calculated [28, 30] for Pd, Pd_2 and larger clusters trapped at the various centres.

The clear result from figure 4 is that trapping at the F_s centre is insufficiently strong to reproduce the high temperature experimental results, essentially due to the small calculated trapping energy E_{2t} = 0.57 eV given in Table IV. At low temperatures, the critical nucleus size i = 1, then 2 (earlier for smaller E_d), but the predicted density curves fall away abruptly from the constant trap density once i = 3. In the calculation for figure 4, we used E_{2t} = 0.65 eV, the binding energy of trapped Pd_3 (with respect to trapped Pd plus two free adsorbed Pd atoms) was taken as 1.40 eV. Pd_4 is stable throughout the T^{-1} range shown, with a corresponding binding

energy of 2.8 eV [30]. As seen in Table IV, the single Pd adatom is calculated to be trapped in the F_s centre with the very high trapping energy of ~2.6 eV; two values have been used for figure 4, 2.60 eV and 1.40 eV; even the smaller of these is sufficient to ensure negligible de-trapping even at the highest temperatures illustrated.

On the other hand, figure 5 shows remarkable agreement with experiment for trapping at the F_s^+ centre. Here we have preferred the value 1.22 eV for the trapped dimer from the periodic model [30, Table 2] to the embedded cluster value 0.91 eV given in Table IV. The additional energies of trapped Pd_3 and Pd_4 were estimated as 0.87 and 1.54 eV respectively [30, Tables 1 and 3]. The calculations for figure 5 used the sums of these values rounded to the nearest 0.05 eV, namely 1.20, 2.05 and 3.60 eV for trapped Pd_2, Pd_3 and Pd_4. Curves are presented for two trapping energies of the Pd monomer, 1.20 and 1.40 eV; the former is close to that calculated in ref [28] by the embedded cluster method, and the latter by the periodic model [30, Table 2]. It can be seen that these "predictions" form an excellent fit to the experimental data, with the diffusion energy E_d between 0.3 and 0.4 eV; that this is identical to a previous DFT value 0.34 eV [28] must be considered fortuitous, as discussed in section 4.3.

The implications of trapping by divacancies are illustrated in figure 6. Here we have a moderately trapped Pd monomer with E_t = 1.64 eV from Table IV [28], rounded to 1.65 eV in our calculation here. Using rounded published values [28, 30], namely 1.70, 2.35 and 3.40 eV for Pd_2, Pd_3 and Pd_4 trapped at the divacancy, we find that the break from the constant trap density corresponds to $i = 4$, and calculated curves are slightly steeper than in figure 5; as a consequence the experiments are not quite so consistent with a unique value of E_d; but the divacancy is certainly not ruled out as a possible candidate from these comparisons with experiment.

On figures 4-6 the further fall-off at the highest temperatures is due to re-evaporation, E_a = 1.35 eV, in line with the calculated values of the adsorption energy on the terrace in both Tables III and IV [18, 20, 28]. Some experimental values deduced for this quantity are lower, around 1.0 eV [2, 32]. But such a low value has a dramatic influence on the prediction if all other values are kept the same. This feature is shown on figure 6, where the near vertical fall of the dashed curves corresponds to the onset of incomplete condensation combined with a large value of $i \geq 4$.

With only 4 clusters included in the prediction, it is not convincing that it the critical size i remains equal to 4 up to the highest temperatures studied. In this situation there are two possible ways forward: either we investigate in detail the energies and other properties of n= 5, 6, etc Pd_n

clusters, or we see what binding energy such clusters would need to be, to change conclusions. This latter approach has been taken with $n \leq 12$, where all clusters above n = 4 have an additional constant binding energy ΔE. We find that $i = 4$ remains if $\Delta E \geq 1.6$ eV, but for $\Delta E \leq 1.5$ eV the critical size grows to $i \geq 12$ at the highest temperatures shown in figure 6.

These values of ΔE are reasonable, but subtle, in that the sublimation energy L of bulk Pd is known from vapour pressure data [33] to be $L = 3.79 \pm 0.1$ eV/atom, and each condensing atom in the repeatable step of the f.c.c. lattice is 6-fold coordinated; this means that the average "energy per bond" in bulk Pd is ~0.63eV. In our case the additional binding energy per Pd atom in the cluster is typically 3-fold coordinated with the cluster, or is 2-fold coordinated and also adsorbed on the substrate. Decreasing additional binding energy with increasing coordination is typical of metallic binding [34], so the condition on ΔE is $\Delta E \geq L/2 - E_a = 0.55\text{-}0.9$ eV in the first case (for the limits on E_a, $1.0 \leq E_a \leq 1.35$ eV) and $\Delta E \geq L/3 = 1.25$ eV in the second. A more realistic figure for 3-fold coordination, based on an analogy with Ag/Ag(111) [35] would be $\Delta E = 0.75L - E_a = 1.5\text{-}1.85$ eV or $\Delta E = L/2 = 1.9$ eV in the second case. The clear implication is that adsorption energies in this range lead to a competition between initial 2D and 3D growth that depends on details of small cluster free energies and associated kinetics.

4.3 Entropic effects on nucleation density predictions

Our assumption in the analysis presented so far is that energies dominate the predictions, and that pre-exponential factors only need to be approximately correct for meaningful predictions to be made. Nonetheless, the nucleation model used also contains a) statistical weights C_j for small clusters j that can have more than one configuration [7, equation 2.7]. Thus we can extend the simplest idea of a dominant cluster configuration with energy E_j, with a sum over configurations m, $\sum_m C_j(m)\exp(E_j(m)/kT)$, replacing the single exponential $C_j\exp(E_j/kT)$. By estimating the configurational entropy, we can come up with revised effective values for C_j.

The model also contains atomic vibration frequencies, so that it can also give the equilibrium vapour pressure at high temperatures [7, section IIIB]; in figures 4-6 the vibration frequency, $\nu = \nu_b$ is that appropriate to bulk Pd sublimation, 3 THz. When applied to adsorbed layers we have in principle three vibration frequencies that can all be different. We have made some predictions here with changed pre-exponential factors, including reducing the (lateral) diffusion frequencies ν_d while fixing the adsorption frequency (ν_a) so as to agree with calculated vertical

vibration frequency [18, 28]; the remaining degrees of freedom (e.g. motions within clusters) are kept at the bulk frequency ν_b. The mean effect of such changes is to shift predicted diffusion energies by up to 0.05 eV in the direction of smaller values, as illustrated in figure 7. These changes are thus interesting, but typically considerably smaller than changes in energies, especially when the uncertainty in energy values is ~±0.1 eV.

Figure 7(a) illustrates the effect of statistical weights for clusters up to n = 4 for the divacancy model of figure 6. Here we have used C_j = [1 0.5 3 5] as a vector for the corresponding four clusters, and 10 for the larger clusters n ≤ 12. The trapped Pd_2 is entropically disfavoured, due to the constrained geometry in the divacancy, whereas the lowest energy Pd_3 trimer is somewhat favoured, due to configurational weight and a possible extra rotational degrees of freedom; similar considerations yield a moderate extra entropy for the Pd_4 tetramer. The details are outlined in the Appendix, but here we only want to extract the approximate size of the effect on the nucleation density. From Figure 7(a) we can see that these entropic effects increase the nucleation density somewhat, and experimental agreement would require E_d to be reduced by ΔE_d ~ 0.03 eV. This is less than the accuracy of our model and so does not change our conclusions.

Figure 7(b) illustrates the similar effects for the F_s^+ centre model of figure 5. Here we have used C_j = [1 5 10 5] as a vector for the corresponding four clusters. Now the trapped Pd_2 is entropically favoured, due to the open geometry (see Appendix), and the two different Pd_3 trimers with similar energy that may have substantial entropy; the Pd_4 tetramer is similar to the previous example. In addition we have changed the adsorption frequency ν_a = 4.0 THz, and lowered the diffusion frequency ν_d = 0.8 THz, while keeping ν_b = 3.0 THz (the default value for all these frequencies before). These entropic effects move the comparison with experiment by ΔE_d ~ 0.05 eV in the complete condensation regime, but have a somewhat larger effect on the onset of incomplete condensation. This means that the value of the adsorption energy needs to be reduced by ΔE_a up to ~0.15 eV for agreement at high temperature; the reason is simply that the adsorbed layer is stabilised by entropic effects related to ν_d that are contained in the original model [7, section III B]. However, both of these effects are at the edge of the accuracy of our model and so do not change our qualitative conclusions. Nonetheless, we can see from figure 6(b) and figure 7(b) that our model does not support a value of E_a as low as 1.0 eV.

5. Discussion and Conclusions

We have discussed recent calculations of adsorption, diffusion, and trapping of some metal adatoms and small clusters on MgO(001), and used these calculations as input for rate equation models of the nucleation density of small metal particles, primarily at defect sites. As a result of comparison with a single experimental data set for Pd/MgO(001) [6], we can effectively rule out the F_s centre as the nucleating agent, and we obtain impressive agreement with nucleation on the F_s^+ and divacancy centres, based on a very extensive set of calculations for Pd/MgO(001) [28-30]. This means that both centres must be considered as candidate defects for nucleation on the MgO(001) surface in general. Of course, this does not rule out the effectiveness of the F_s centre at lower temperatures, if the defect were present, but the implication is that it was not the dominant defect in relation to ref [6].

This paper also opens the way for other experiment-theory comparisons of metals on MgO and other (ionic) crystal surfaces. The limiting requirement is that good data sets of nucleation density are available, and that reliable energy calculations have been, or can be, performed on several small clusters. Ironically, there is already a large data set available for the same metal combination as studied here, Pd/MgO(001) [2, 32], which *cannot* be fitted with the same defect parameters, but which parallels the behavior of Au/MgO(001) [36]. Since the only real difference between these studies and our experimental data set [6] is the method of surface preparation, it is now logical to explore whether there are other surface defects, and possibly other surface processes such as dimer mobility, that could explain these reproducible results. A recent theoretical study has made a serious start in this direction [37].

There are of course other developments in the modeling of nucleation and growth at defect sites in addition to those presented here. The model given is a mean field model, aimed primarily at identifying important energies, but also being able to discuss entropic effects as in section 4.3. In parallel, other authors are developing descriptions of cluster size distributions [11, 38], which may be used to extract further information from experiment-theory comparisons in future. Such developments may be useful if sufficiently detailed experimental results and *ab-initio* calculations become available.

Acknowledgments

This paper arose as a result of an invitation to present a paper at a special meeting in June 2005 in London in honour of the career of Marshall Stoneham. It is a pleasure to thank Andrew Fisher for this invitation, and to thank Marshall for encouraging the first author to collaborate with his group at UCL over the last decade, especially with John Harding, and for discussions on this paper. At the meeting the emphasis of John Venables' talk was on discrepancies in the theoretical literature for the energies of small metal clusters on MgO, and how maybe to resolve them using the recent work of the Pacchioni group in Milan. At the same meeting, the first author learned from Alex Shluger that the second author, Livia Giordano, would be visiting him at UCL for a month in July-August. So, a few trips from Sussex to London later, we have a paper; it's a small world! Livia thanks Alex Shluger (via EPSRC grant GR/S80080/01) and Gianfranco Pacchioni (via the European STREP project GSOMEN) for supporting her stay in London. John Harding acknowledges EPSRC for support under grant GR/R85969.

Appendix: What is a reasonable configurational entropy for small clusters?

We are interested here in rough order of magnitude arguments. We already have Einstein vibrations in our model [7], but the additional entropy due to position may perhaps be as much as in a liquid. A typical liquid entropy, e.g. for bulk Pd is $L_m = T_m \Delta S$, so we can work out ΔS and apply it at the condensation temperature. Honig and Kramer [33] give L_m = 4.2 kcal/mol = 4200/1.987 K/atom , and T_m = 1825 K. So L_m = 2114 K/atom = 0.182 eV, and ΔS = 2114/1825 = 1.16 in k_B units, which is in the typical liquid range,1-2k/atom.

Therefore for monomers we already have all the degrees of freedom, unless we have a 2D gas, but we can investigate the effect of reducing ν_d, as in figure 7(b). The value, ν_d = 0.8 THz, was estimated by assuming the potential along the <110> jump direction is a sine curve with amplitude $E_d/2$, based on E_d = 0.25 eV; the consequences are spelt out in the text.

For dimers in the F_s^+ centre we should have C_2 = 4, from the geometry of the lattice, and $\exp(\Delta S/k) = \exp(1.16) = 3.19$. So C_2 in the range 4-8 is certainly possible, and we choose 5 for illustration. For the divacancy, there is only one configuration, and that may have restricted, i.e. high energy, vibrations. So C_2 may well be < 1, and we choose 0.5 for illustration.

For C_3, we know we have 2 trimer configurations on an F_s^+ centre that are low-lying in energy (F1 and F2 [30, figure 5], as shown here in figure 5(a)), and each of these have several

possible equivalent arrangements. The F1 centre must have 4 configurations and the F2, 4 also. So $C_3 = 8$ from this argument and is ~ $(3.19)^2 = 10.2$ from the liquid argument; we choose $C_3 = 10$ for illustration. For the divacancy, the energies of different configurations are dissimilar, so we consider D1 only [30, figure 4], shown here in figure 6(a). From symmetry (mirror about the divacancy axis) this looks like $C_3 = 2$, anyway not very large; the trimer could have a measure of free rotation about one axis. This gives an additional $\Delta S = k/2$, and so $C_3 = 2\exp(0.5) = 3.3$. We choose $C_3 = 3$ for illustration.

For C_4, we again have rather different energies, so that the F_s^+ centre (F1) has $C_4 = 4$, whereas the liquid model would give $(3.19)^3 = 32.5$. But given the approximate symmetry of this cluster, it looks like free rotation may be possible; if there isn't free rotation, then the smaller value may be better. So let's assume we have free rotation of a triplet of atoms around a single axis, and hence $C_4 = 4\exp(0.5) = 6.6$. For the divacancy, D1 and D2 [30, figure 8] are close in energy, so consider both; there are just 2 conformations of each by symmetry. Both configurations have one atom close to the Mg ion vacancy and tend to avoid the O ion vacancy. So let's assume we have free rotation of a triplet of atoms around a single axis. This gives $C_4 = 2*2\exp(0.5) = 6.6$ also. Anything around this value is reasonable, and we choose $C_4 = 5$ for illustration.

References

[1] Campbell C T (1997) Surface Sci. Rep. **27** 1

[2] Henry C R (1998) Surface Sci. Rep. **31** 231

[3] Pacchioni G (2001) in Oxide Surfaces, *The Chemical Physics of Solid Surfaces, vol 9* (Ed. Woodruff D P, Elsevier, Amsterdam) 94

[4] Harding J H, Stoneham A M and Venables J A (1998) Phys. Rev. B **57** 6715

[5] Venables J A and Harding J H (2000) J. Cryst. Growth **211** 27 and references quoted.

[6] Haas G, Menck A, Brune H, Barth J V, Venables J A and Kern K (2000) Phys. Rev. B **61** 11105

[7] Venables J A (1987) Phys. Rev. B **36** 4153

[8] Venables J A (1994) Surface Sci. **299/300** 798 and references quoted

[9] Brune H (1998) Surface Sci. Rep. **31** 121

[10] Venables J A, Bennett P A, Brune H, Drucker J and Harding J H (2003) Phil. Trans. R. Soc. Lond. A **361** 311

[11] Ratsch C and Venables J A (2003) J. Vac. Sci. Tech. A **21** S96

[12] Balasubramanian K (1988) J. Chem. Phys. **89** 6310

[13] Beute V, Kramer H G, Kuhn M, Weyers W and Demtroides W (1993) J. Chem. Phys. **98** 2699

[14] Yudanov I V, Pacchioni G, Neyman K and Rösch N (1997) J. Phys. Chem. B **101** 2786

[15] Neyman K M, Vent S, Pacchioni G and Rösch N (1997) Nuovo Cimento **19D** 1743

[16] Spiess L (1996) Surface Rev. Lett. **3** 1365

[17] Ferrari A M and Pacchioni G (1996) J. Phys. Chem. **100** 9032

[18] Matveev A V, Neyman K M, Yudanov I V and Rösch N (1999) Surface Sci. **426** 123

[19] Bogicevic A and Jennison D R (1999) Surface Sci. **437** (1999) L741

[20] Bogicevic A and Jennison D R (2002) Surface Sci. **515** (2002) L481

[21] Shim I and Gingerich K A (1984) J. Chem. Phys. **80** 5107

[22] Gingerich K A, Shim I, Gupta S K and Kincade J E, Jr (1985) Surface Sci. **156** 495

[23] Morse M D (1986) Chem. Rev. **86** 1049

[24] Harada M and Dexpert H (1996) J. Phys. Chem. **100** 565

[25] Valerio G and Toulhoat H (1996) J. Phys. Chem. **100** 10827

[26] Seminario J M, Zacarías A G and Castro M (1997) Int. J. Quant. Chem. **61** 515

[27] Fuks D, Dorfman S, Zhukovskii Y F, Kotomin E A and Stoneham A M (2002) Surface Sci. **499** 24

[28] Giordano L, Di Valentin C, Goniakowski J and Pacchioni G (2004) Phys. Rev. Lett. **92** 096105

[29] Giordano L, Di Valentin C, Pacchioni G and Goniakowski J (2005) Chemical Phys. **309** 41

[30] Giordano L and Pacchioni G (2005) Surface Sci. **575** 197

[31] Sushko P V, Shluger A L and Catlow C R A (2000) Surface Sci. **450** 153

[32] Henry C R and Meunier M, Vacuum **50** (1998) 157

[33] Honig R and Kramer D A (1969) RCA Review **30** 285

[34] Jacobsen K W, Nørskov J K and Puska M J (1987) Phys. Rev. B **35** 7423

[35] Jones G W, Marcano J M, Nørskov J K and Venables J A (1990) Phys. Rev. Lett. **65** 3317

[36] Højruop-Hansen K, Ferrero S and Henry C R (2004) Appl. Surface Sci. **226** 167

[37] Del Vitto A, Pacchioni G, Delbecq F and Sautet P (2005) J. Phys. Chem. B **109** 8040

[38] Vardavas R, Ratsch C and Caflisch R E (2004) Surface Sci. **569** 185

[39] A. Bogicevic (2005) private communication

Table I:

Calculated adsorption energy (eV) of Pd and Ag on MgO (001)

Pd [ref]	[5]	[14-15]	Ag [ref]	[5]	[16]
Pd over O^{2-}	0.85	0.81	Ag over O^{2-}	0.66	0.66
over Mg^{2+}	0.24	0.59	over Mg^{2+}	0.22	0.36
over hollow	0.58	0.58	over hollow	0.56	0.53

Table II:

Calculated adsorption and diffusion energies (eV) of monomers and dimers on MgO (001)

Pd [5]	E_a	E_d	E_d [15]	Ag [5]	E_a	E_d	E_d [16]
Monomer	0.85	0.2	0.23	Monomer	0.66	0.1	0.13
Dimer	1.47	0.3		Dimer	1.27	0.3	

Table III:

Comparisons of E_a, E_b, E_t and E_{2t} (eV) for Pd, Pt, Ag and Au on MgO(001)

	Ads: E_a	*F* trap: E_t	Bind: E_b	*D* trap: E_{2t}
Pd	1.34 (1.35)	2.72 (2.55)	–0.03	0.09
Ag	0.53 (0.41)	1.27 (1.31)	1.81	1.86
Pt	2.67	3.83	0.72	–0.14
Au	0.90	2.22	2.15	2.21

DFT spin-unpolarised calculations from refs [19, 20], except for the values in round brackets, which are for a spin-polarised DFT-GGA embedded cluster calculation [18]. Ads: Adsorption on the perfect terrace; *F* trap: an adatom at the F_s centre; Bind: Binding energy of a dimer on the terrace; *D* trap: a dimer at the F_s centre.

Table IV:

DFT-GGA spin-polarised model: Energies (eV) of Pd and Pd_2 on MgO(001)

	Terrace	Step	OH [29]	F_s	F_s+	DiVac
Pd (E_a)	1.36 (1.35)	1.85	2.70	3.99 (3.90)	2.70 (2.62)	3.00
trap (E_t)		0.49	1.31	2.63 (2.55)	1.20 (1.27)	1.64
Pd_2 (E_{dim})	1.86	2.02	2.73	1.93	2.41	3.06
trap (E_{2t})	0.50 (E_b)	0.66	1.34	0.57	0.91	1.71

Periodic slab model from ref [28], except where noted, see text for discussion. The F_s^+ values are for an embedded cluster calculation in ref [28]. The values in round brackets are for a spin-polarised DFT-GGA embedded cluster calculation in ref [18]. Terrace: Adsorption on the 5-fold coordinated terrace; Step (OH): an adatom or dimer at a 4-fold coordinated step (containing an OH group); F_s, (F_s^+): an adatom or dimer at the neutral F_s (singly charged F_s^+) centre; DiVac: an adatom or dimer at a neutral di-vacancy. The trapping at the OH ion, at a step, is from ref [29].

Figure Captions

Figure 1: Model for nucleation at randomly placed point defects with variables n_1: number density of free adatoms; n_t: density of traps; n_{1t}: density of trapped adatoms; and n_{xt}: density of trapped stable clusters (clusters with atom numbers > i). The total density of stable clusters (trapped and free) is n_x. See text for discussion.

Figure 2: Arrhenius representation of Pd island density N_x (cm^{-2}) at 0.1 ML coverage on Ar-cleaved Mg(001): The solid line is the model for E_d = 0.2, E_t = 1.5, E_b = 1.2 and E_a = 1.2 eV, plus curves for E_d = 0.3 (dashed) and 0.4 eV (dotted lines), and experimental data from [6]. The insert shows the model for i = 3 applicable at high temperatures, using the same notation as figure 1, after [10]; See text for discussion.

Figure 3: a) Nucleation density predicted with trap density n_t = 2.65x10^{-3} ML, E_d = 0.2 eV, E_a and E_b = 1.2 eV, and various values of trap energy E_t, as indicated; b) Nucleation density predicted with n_t = 2.65x10^{-3} ML, E_d = 0.2 eV, E_t = 1.5 eV and E_a = 1.2 eV, for two values of the lateral pair binding energy E_b = 1.0 and 1.2 eV. The data points involving incomplete condensation are indicated by triangles, complete condensation by squares, as in figure 2. See text for discussion.

Figure 4: Predictions using F_s trapping parameters for Pd_n clusters (n = 1 to 4) and adsorption energy E_a from [28, 30]: a) Clusters considered, including two types of trimer [30]; b) Nucleation density and *i*-sizes as a function of 1000/*T*, with parameter E_d. See text for discussion.

Figure 5: Predictions using F_s^+ trapping parameters for Pd_n clusters (n = 1 to 4) and adsorption energy E_a and two values of the trapping energy E_t from [28, 30]: a) Clusters considered, including two types of trimer, F1(left) and F2 (right) [30]; b) Nucleation density and *i*-sizes as a function of 1000/*T*, with parameter E_d. See text for discussion.

Figure 6: Predictions using divacancy trapping parameters for Pd_n clusters (n = 1 to 4) [28, 30], with additional energies ΔE = 1.6 eV for n = 5 to 12. a) Clusters considered explicitly [30]; b) Nucleation density and *i*-sizes as a function of 1000/*T*, with parameter E_d. The trapping energy E_t = 1.35 eV, with two values of E_a, 1.35 eV from [18, 28], and the lower value 1.0 eV to illustrate the dramatic effect of incomplete condensation when all other parameters are kept the same. See text for discussion.

Figure 7: Predictions illustrating the effects of changes in pre-exponential factors, using calculated trapping parameters for Pd_n clusters (n = 1 to 4) from [28, 30] a) inclusion of statistical weights C_j = [1 0.5 3 5] into the divacancy model of figure 6. All other parameters remain the same, including the value of ΔE for n > 4; b) inclusion of statistics C_j = [1 5 10 5], and changed frequency factors into the F_s^+ model of figure 5, for two values of the adsorption energy E_a = 1.35 and 1.20 eV, all other parameters remaining the same. See text for discussion.

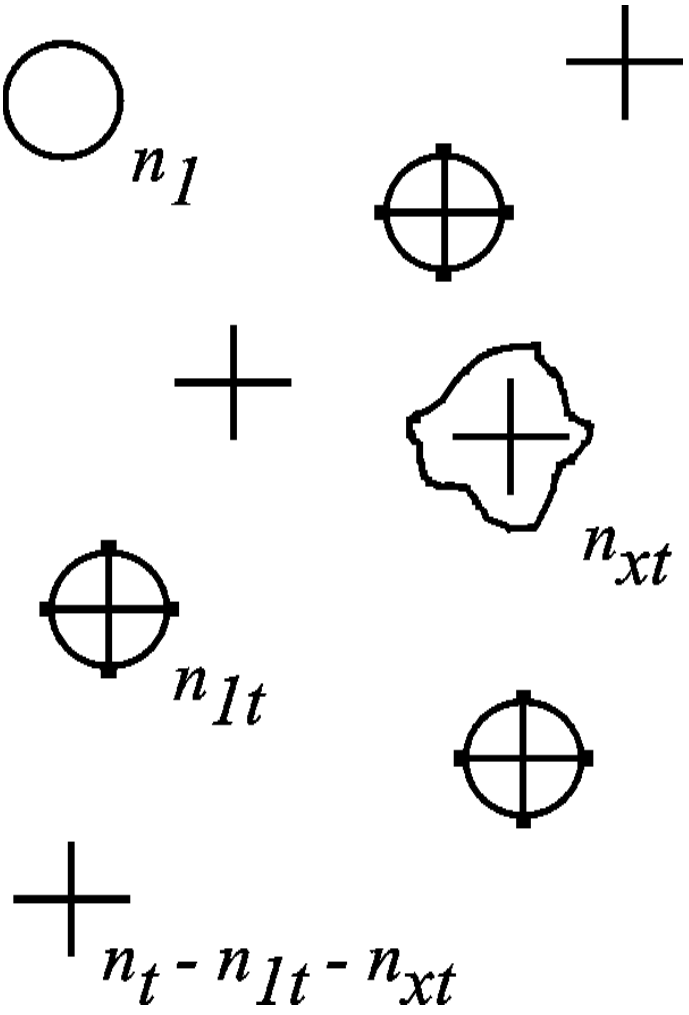

Fig. 1: Model for nucleation at randomly placed point defects with variables n_1: number density of free adatoms; n_t: density of traps; n_{1t}: density of trapped adatoms; and n_{xt}: density of trapped stable clusters (clusters with atom numbers > i). The total density of stable clusters (trapped and free) is n_x. See text for discussion.

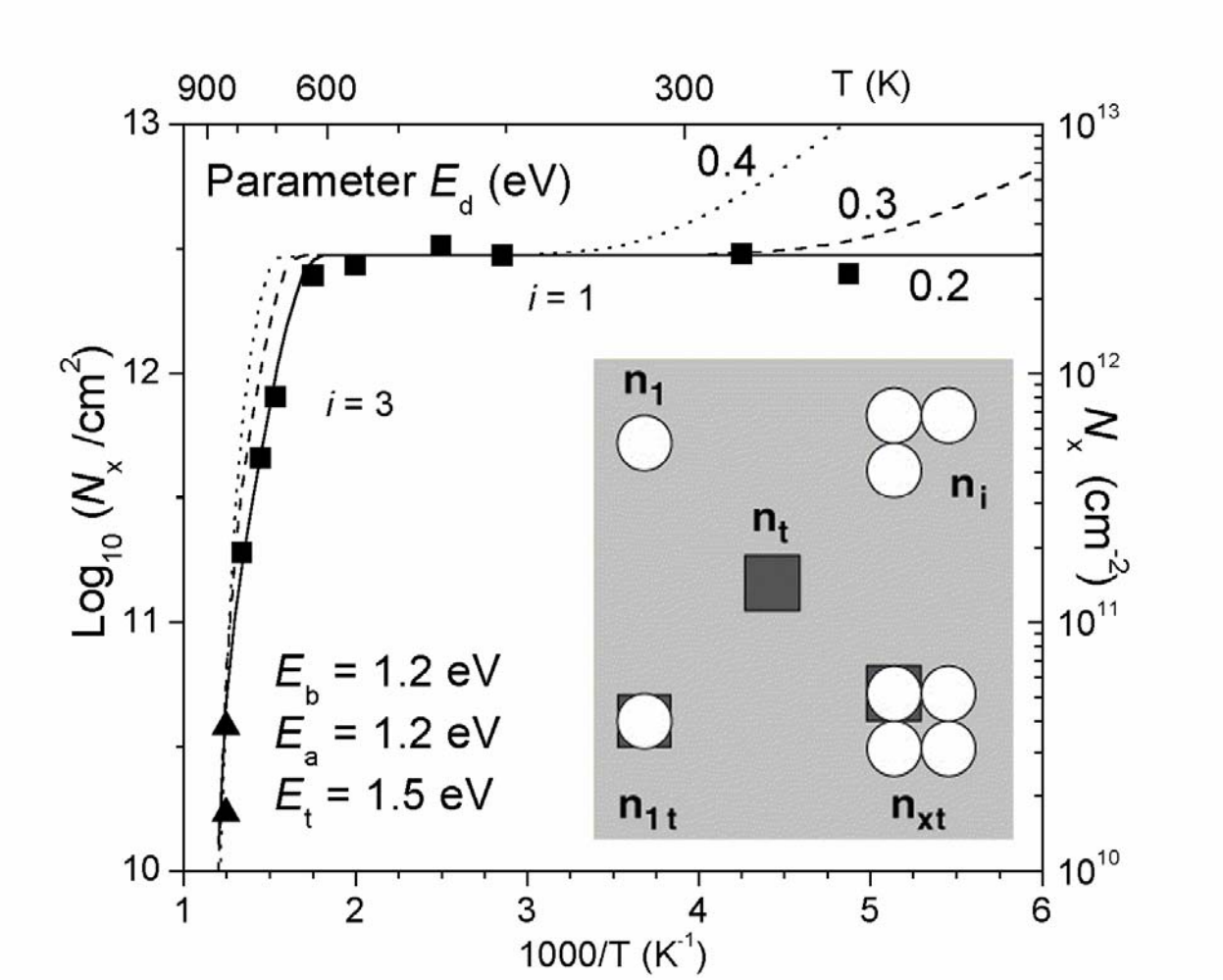

Figure 2: Arrhenius representation of Pd island density N_x (cm^{-2}) at 0.1 ML coverage on Ar-cleaved Mg(001): The solid line is the model for E_d = 0.2, E_t = 1.5, E_b = 1.2 and E_a = 1.2 eV, plus curves for E_d = 0.3 (dashed) and 0.4 eV (dotted lines), and experimental data from [6]. The insert shows the model for i = 3 applicable at high temperatures, using the same notation as figure 1, after [10]; See text for discussion.

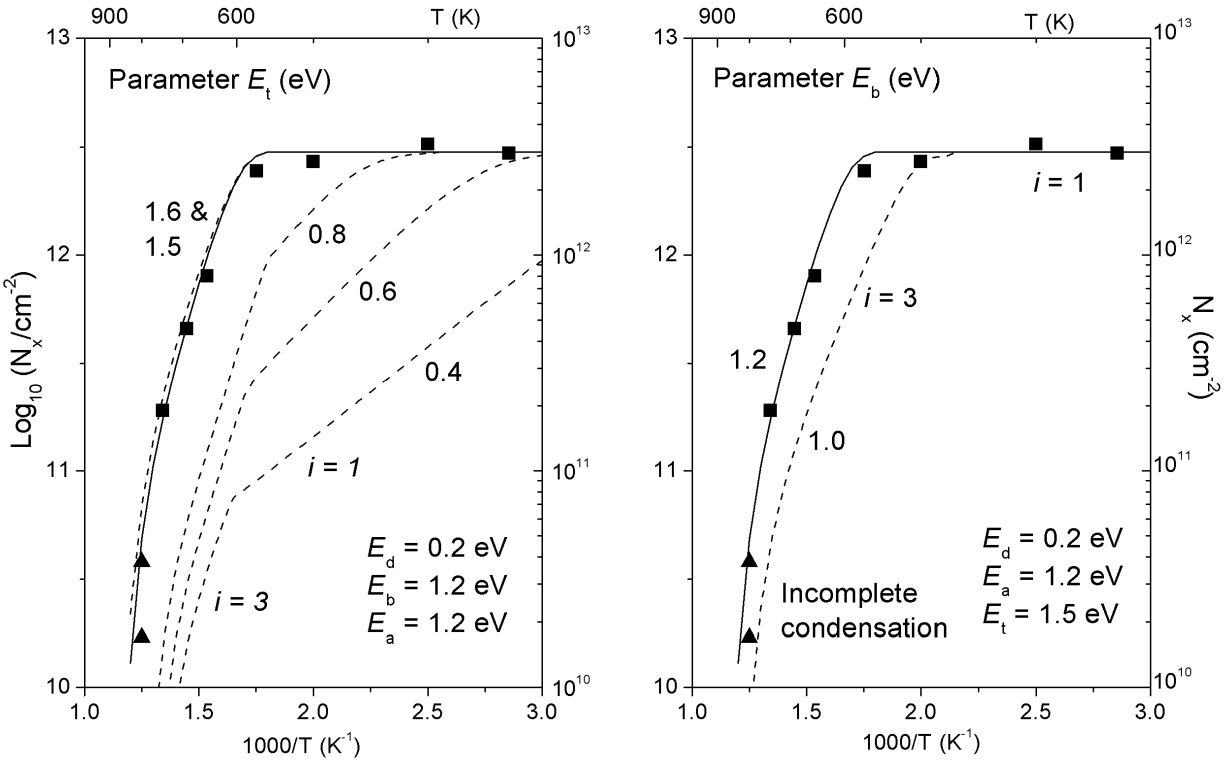

Figure 3: a) Nucleation density predicted with trap density n_t = 2.65x10^{-3} ML, E_d = 0.2 eV, E_a and E_b = 1.2 eV, and various values of trap energy E_t, as indicated; b) Nucleation density predicted with n_t = 2.65x10^{-3} ML, E_d = 0.2 eV, E_t = 1.5 eV and E_a = 1.2 eV, for two values of the lateral pair binding energy E_b = 1.0 and 1.2 eV from ref [5]. Higher values of E_a lead to increased slope, but only at the highest temperatures. The data points involving incomplete condensation are indicated by triangles, complete condensation by squares, as in figure 2. See text for discussion.

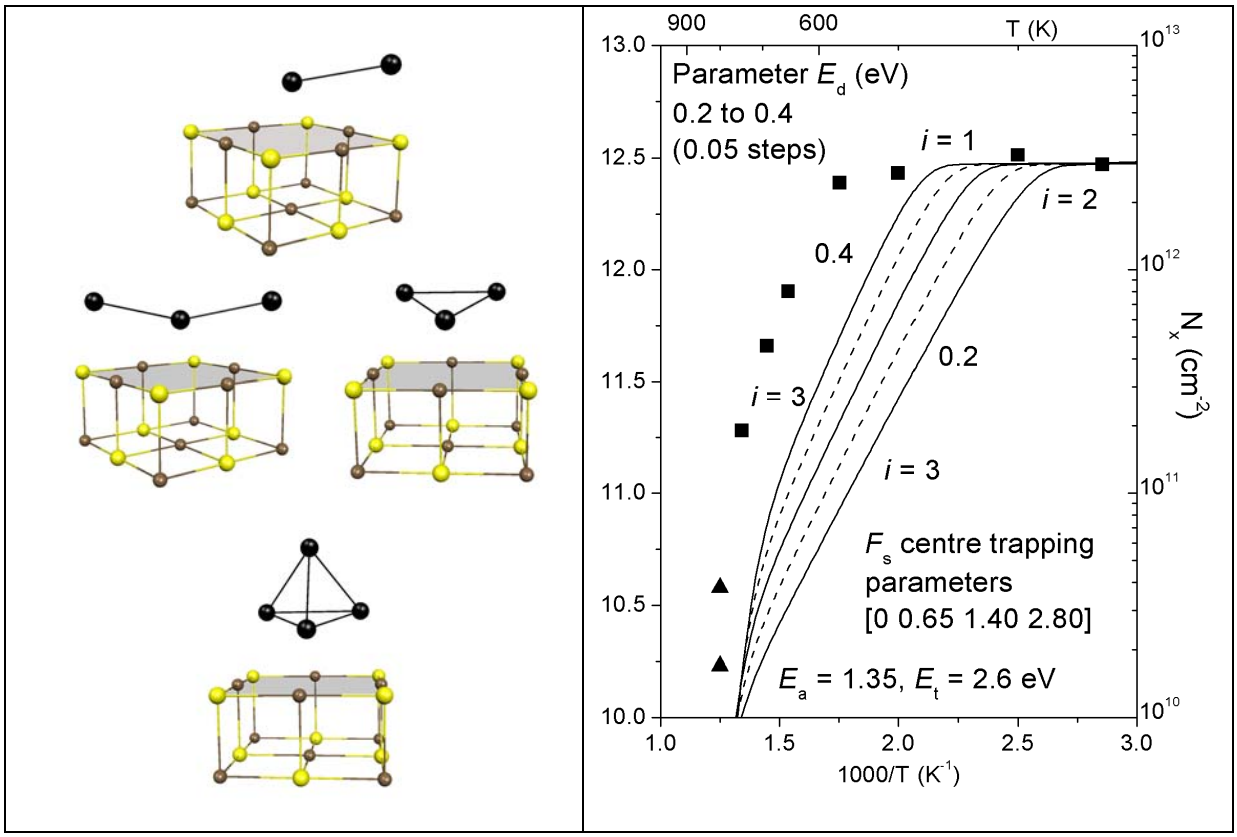

Figure 4: Predictions using F_s trapping parameters for Pd_n clusters (n = 1 to 4) and adsorption energy E_a from [28, 30]: a) Clusters considered, including two types of trimer [30]; b) Nucleation density and *i*-sizes as a function of 1000/*T*, with parameter E_d. See text for discussion.

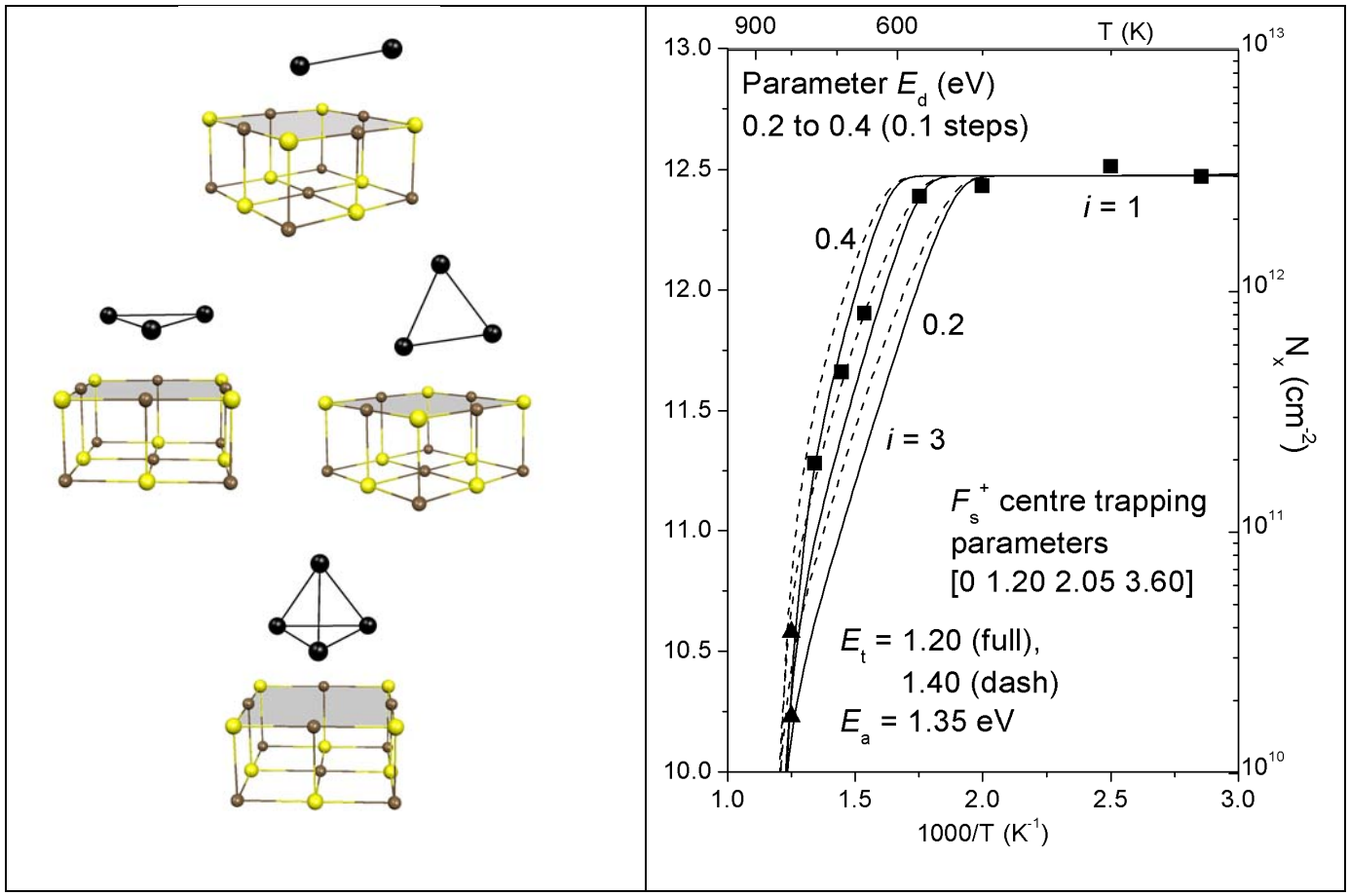

Figure 5: Predictions using F_s^+ trapping parameters for Pd_n clusters (n = 1 to 4) and adsorption energy E_a and two values of the trapping energy E_t from [28, 30]: a) Clusters considered, including two types of trimer [30]; b) Nucleation density and *i*-sizes as a function of 1000/*T*, with parameter E_d. See text for discussion.

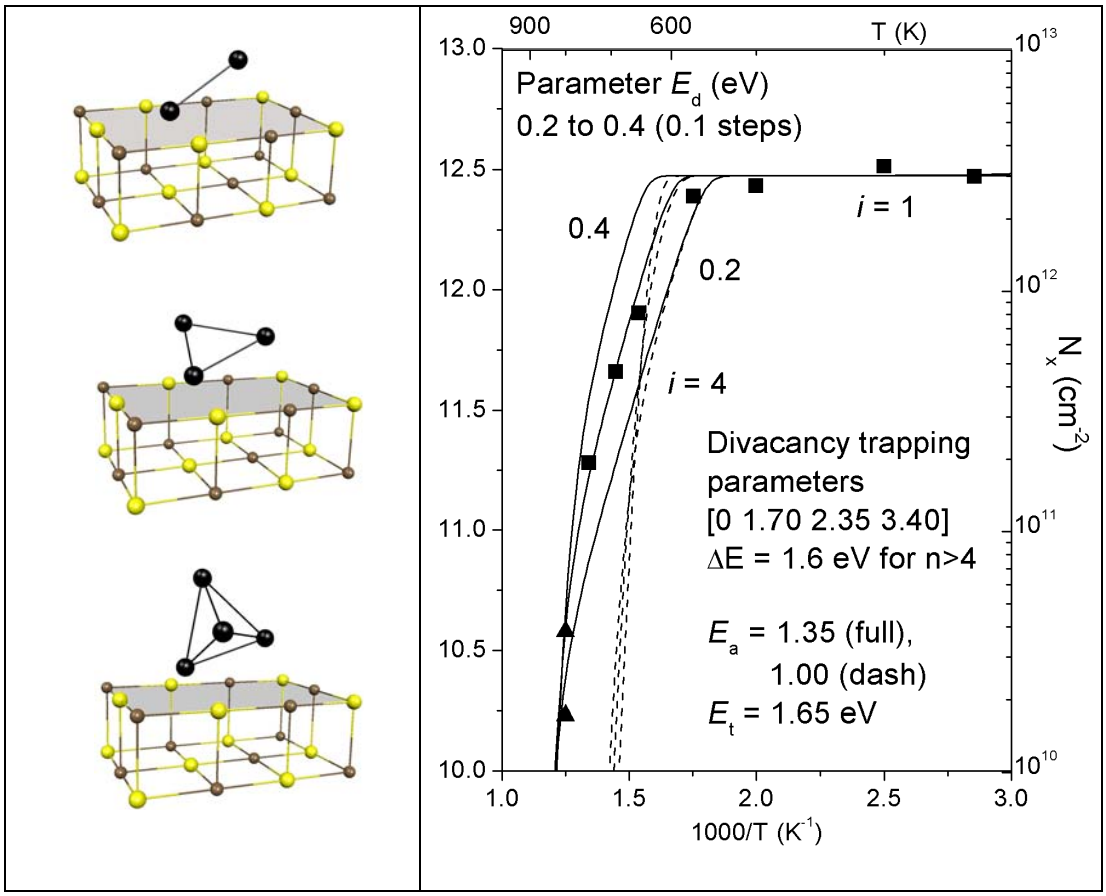

Figure 6: Predictions using divacancy trapping parameters for Pd_n clusters (n = 1 to 4) [28, 30], with additional energies ΔE = 1.6 eV for n = 5 to 12. a) Clusters considered explicitly [30]; b) Nucleation density and *i*-sizes as a function of 1000/*T*, with parameter E_d. The trapping energy E_t = 1.35 eV, with two values of E_a, 1.35 eV from [18, 28], and the lower value 1.0 eV to illustrate the dramatic effect of incomplete condensation when all other parameters are kept the same. See text for discussion.

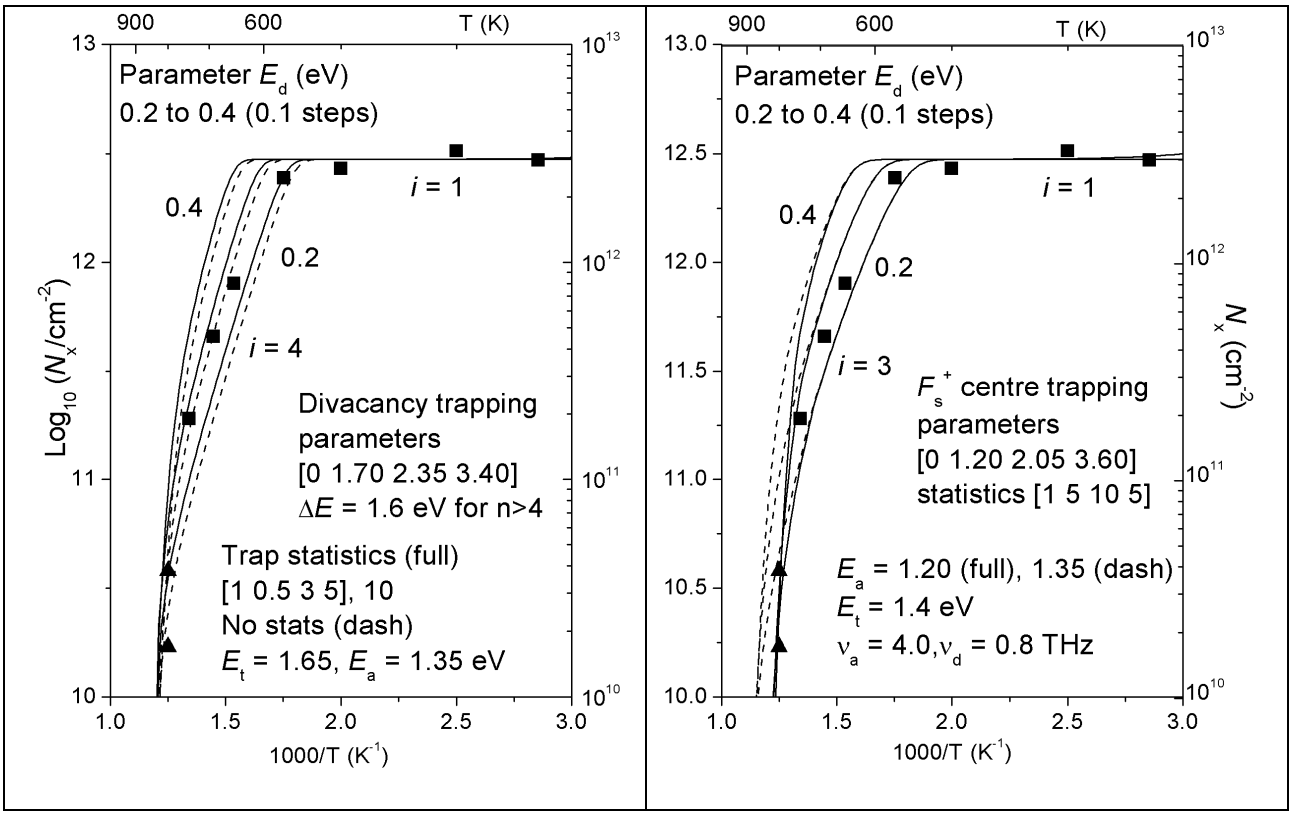

Figure 7: Predictions illustrating the effects of changes in pre-exponential factors, using calculated trapping parameters for Pd_n clusters (n = 1 to 4) from [28, 30] a) inclusion of statistical weights *C*j = [1 0 10 5] into the divacancy model of figure 6. All other parameters remain the same, including the value of ΔE for n > 4; b) inclusion of statistics *C*j = [1 3 10 5], and changed frequency factors into the F_s^+ model of figure 5, for two values of the adsorption energy E_a = 1.35 and 1.25 eV, all other parameters remaining the same. See text for discussion.